Mon. Not. R. Astron. Soc. **296,** 483–490 (1998)

B0712+472: a new radio four-image gravitational lens

N. Jackson,[1] S. Nair,[1] I. W. A. Browne,[1] P. N. Wilkinson, [1] T. W. B. Muxlow,[1]
A. G. de Bruyn,[2,3] L. Koopmans,[3] M. Bremer,[4] I. Snellen,[4] G. K. Miley,[4]
R. T. Schilizzi,[4,5] S. Myers,[6] C. D. Fassnacht,[7] D. S. Womble,[7] A. C. S. Readhead,[7]
R. D. Blandford[7] and T. J. Pearson[7]

[1]*University of Manchester, NRAL Jodrell Bank, Macclesfield, Cheshire SK11 9DL*
[2]*Netherlands Foundation for Radio Astronomy, 7990 AA Dwingeloo, the Netherlands*
[3]*Kapteyn Laboratory, Postbus 800, 9700 AA Groningen, the Netherlands*
[4]*Sterrewacht Leiden, Postbus 9513, 2300RA Leiden, the Netherlands*
[5]*Joint Institute for VLBI in Europe, Postbus 2, 7990 AA Dwingeloo, the Netherlands*
[6]*Department of Physics, University of Pennsylvania, Philadelphia, PA 19104, USA*
[7]*California Institute of Technology, Pasadena, CA 91125, USA*

Accepted 1997 November 3. Received 1997 August 27; in original form 1997 April 18

ABSTRACT

A new four-image gravitational lens system, B0712+472, has been discovered during the Cosmic Lens All-Sky Survey. This system consists of four flat-spectrum radio images that are also seen on a *Hubble Space Telescope* (*HST*) image, together with the lensing galaxy. We present MERLIN, VLA and VLBA maps and WHT spectra of the system as well as the *HST* images. The light distribution of the lensing galaxy is highly elongated and so too is the mass distribution deduced from modelling. We suggest a redshift of ∼1.33 for the lensed object; the lens redshift will require further investigation. The discovery of this new system further increases the ratio of four-image to two-image lens systems currently known, exacerbating problems of required ellipticity of matter distributions in lensing galaxies.

Key words: galaxies: active – galaxies: fundamental parameters – quasars: emission lines – gravitational lensing.

1 INTRODUCTION

The Cosmic Lens All-Sky Survey (CLASS) is a survey of flat-spectrum radio sources the primary purpose of which is the discovery of new radio-loud gravitational lens systems. A survey of 10 000 radio sources is being undertaken; those sources found to contain extended structure in an initial VLA snapshot are examined at higher resolution with MERLIN and the VLBA. Higher resolution allows one to separate the genuine lens systems, which consist of multiple flat-spectrum components, from systems containing a flat-spectrum core and steep-spectrum extended radio emission. The discovery of two lenses, 1600+434 and 1608+656, has already been announced (Jackson et al. 1995; Myers et al. 1995) and a companion paper reports the discovery of another lens, 1933+503 (Sykes et al. 1988).

In this paper we present observations of B0712+472, a new lens system. The radio source was selected owing to a coincidence of a 36-mJy source from the NRAO 5-GHz survey of 1987 October, 87GB 071218.5+47133 (Condon, Broderick & Seielstad 1989) with a 35-mJy source in the 325-MHz Westerbork Northern Sky Survey (de Bruyn et al., in preparation). It was observed during the 3247-source, first phase of the CLASS survey (see Jackson et al. 1995). We present radio maps together with the optical pictures which demonstrate beyond serious doubt the presence of gravitational lensing.

2 RADIO AND OPTICAL OBSERVATIONS

2.1 The radio images

Table 1 gives a log of the observations. The discovery VLA image (Fig. 1, middle left) showed a resolved, brighter component together with a compact secondary 1 arcsec to the south-east. In common with ∼80 other flat-spectrum sources that did not consist of single points, it was followed up using MERLIN at 5 GHz; after this process it was confirmed as a multiple-image gravitational lens candidate.

Radio maps of B0712+472 have been made at two frequencies and with a variety of resolutions, using the NRAO AIPS package and the Caltech DIFMAP software (Shepherd, Pearson & Taylor 1995). The maps made with the VLA and MERLIN (Fig. 1) reveal four components, the brightest three of which are detected in the VLBA observations. No structure in addition to the point components is visible on the 5-mas resolution VLBA maps (Wilkinson et al., in

Table 1. Observations of B0712+472. The observing dates are given, in chronological order, for both radio and optical observations. The resolution in arcsec is the clean beam of the maps in the case of the radio images, or the diffraction-limited resolution in the case of the *HST* images (which is undersampled by the pixel scale of 0.045 arcsec).

Telescope	Obs. date	Exp. time	Frequency or λ	Resolution(arcsec)	Noise level (mJy/beam)
VLA	1994 Mar 02	30 s	8.4 GHz	0.22	0.3
MERLIN	1995 Mar 09	1 hr	5 GHz	0.05	0.25
WSRT	1995 Jun 3	30 min	5 GHz		
VLA	1995 Aug 28	30 min	15 GHz	0.10	0.12
VLBA	1995 Nov 12	35 min	5 GHz	0.005	0.15
WHT	1995 Dec 22	30 min	340-840 nm	Spectrum	
WHT	1995 Dec 23	1 hr	360-880 nm	Spectrum	
HST	1996 Jan 29	800 s	540 nm	0.045	
HST	1996 Jan 29	1000 s	814 nm	0.067	
VLA	1996 Jul 06	300 s	8.4 GHz	0.125	
MERLIN	1996 Nov 15	20 hr	5 GHz	0.05	0.053

preparation) or the >100-mas resolution VLA maps. However, the map produced from the MERLIN 5-GHz long-track (20 h) observation (Fig. 1), which is the deepest radio image, shows hints of emission around the two bright components. There appears to be a faint bridge-like feature between these two components.

The flux densities for the images are listed in Table 2. The radio spectral indices (5–15 GHz) of the three well-detected images do not differ significantly from each other, given the errors in the flux densities.

We can check whether or not the lensed object is variable using our data. The flux densities measured with the VLBA at 5 GHz in 1995 November are very similar to those determined with MERLIN in 1996; however, both sets of flux densities are about 30 per cent less than the MERLIN 1995 flux density (see Table 2). Moreover, we note that the Gregory & Condon (1991) 5-GHz total flux density is 36 mJy, which despite a large error (6 mJy) is not consistent with our 1996 value. The 1995 June 3 Westerbork Synthesis Radio Telescope (WSRT) measurement gave a total flux density of 27 ± 1 mJy, which is also less than the MERLIN total flux density from 1995 March. It is thus likely that all of the images became somewhat fainter during 1995, and that at least some variability happens on time-scales of $\sim$2 months or less. The similarity of the VLBA and MERLIN flux densities makes it unlikely that any of the components are more than $\sim$10–20 per cent resolved (the peak flux in the VLBA map is at least 80 per cent of the MERLIN flux at the same frequency) and must be $\leq$1 mas FWHM.

A polarization image has also been made from the 1996 MERLIN data, but no polarized flux is visible at a (2σ) level corresponding to 1 per cent of the flux of the A component.

The observations presented thus far support the interpretation of A, B and C as gravitationally lensed images of the same source. The fourth image, D, appears repeatedly at the same location at 5 GHz (MERLIN) and 15 GHz (VLA), making it apparent that it is the fourth image in a standard quadruple image configuration. (There is no fifth image to the MERLIN 3σ limit of about 0.15 mJy). The system appears similar in its morphology to the radio-loud lenses MG0414+0534 (Katz & Hewitt 1993), 1422+231 (Patnaik et al. 1992) and 1608+656 (Myers et al. 1995).

2.2 *HST* images

Further confirmation that this is a lensed system is provided by our *HST* images of the system (Fig. 2). The A, B and C images are all clearly visible on the frames taken at both 555 nm and 814 nm. The astrometry of the *HST* image is not good enough to derive absolute optical positions to better than 0.5 arcsec. However, the relative positions of the optical images A, B and C agree with those of the radio image to within the combined error of between 10 and 20 mas, reinforcing the conclusion that we are dealing with a lensed system. The D image is located on the other side of the lensing galaxy from A, B and C, also consistent with the lensing interpretation.

The galaxy responsible for the lensing is clearly visible in the *HST* pictures, and appears as an elongated disc-like system of magnitude 22.2 in *V* and 20.0 in *I* (in elliptical apertures of 2×1 arcsec^2, avoiding the lensed images: the total magnitudes are 21.6 and 19.6 in *V* and *I* respectively). Ellipse fits made using STSDAS/IRAF software require an ellipticity ($1 - b/a$) of between 0.4 and 0.5 along semi-major axes around 0.5 arcsec from the centre of the galaxy. However, the galaxy has a central core, with ellipticities of <0.2 within the central 0.2 arcsec. The position angle, of $60° \pm 5°$, agrees very well with the best-fitting model (Section 4) of 50.6°.

We can also investigate the morphology of the lensing galaxy in an attempt to identify its Hubble type. The most significant factors are its high ellipticity and the lack of dominance of the central condensation: the concentration index (*CI*), defined by Driver, Windhorst & Griffith (1995), is -1.3 for the galaxy (Jackson et al. 1997), which is outside the range ($CI < -2$) normally occupied by elliptical galaxies (Driver et al. 1995). Moreover, we argue elsewhere (Jackson et al. 1997) that concentration measures (Abraham et al. 1994, 1995, 1996) also suggest an identification as an Sa or later type. However, profiles of the galaxy from the *I*-band image (Fig. 3), with the images of the lensed object blanked out, suggest an $r^{1/4}$ law fits better the isophotes in the inner bulge, (although note that the isophotes are disturbed at around 0.8 arcsec by the blanking required to remove the lensed images). There is thus not overwhelming evidence for identification as a spiral or as an elliptical. The $V - I$ colour of the galaxy is $\sim$2.2, which is approximately that of an S0/Sa galaxy at a redshift of 0.5 (Fukugita, Shimasaku & Ichikawa 1995). However, if the redshift were 0.3, the colour alone would indicate an identification as an elliptical. Owing to the large intrinsic scatter in colours of galaxies and our ignorance of the lens redshift we are unable to make a definite statement based on the colour.

There may be fuzz visible around the images of the lensed object, in particular image C; however this is marginal and requires confirmation. What is surprising is the faintness of the optical images; the total magnitude of all four added together is $\sim$23 in *V*.

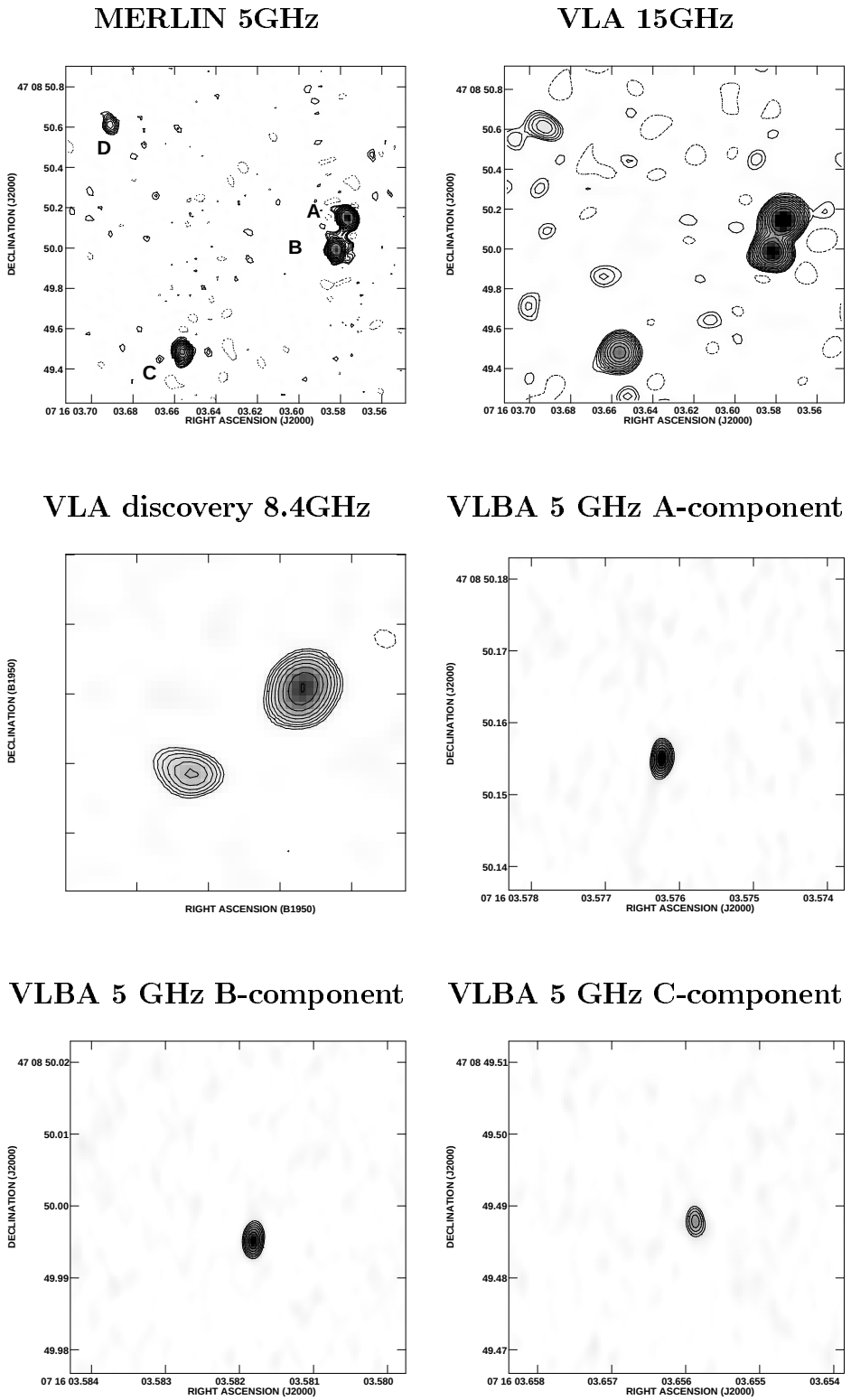

Figure 1. Radio images of the B0712+472 system. Top left: MERLIN 20-h 5-GHz image (naturally weighted; lowest contour level is 120 μJy; the beam is 60×44 mas^2 in PA 18°). Top right: VLA 15-GHz image (beam 0.1 arcsec; lowest contour level 200 μJy). Middle left: Original VLA 8.4-GHz discovery image (lowest contour level 1 mJy). Middle right: VLBA image of component A. Bottom, left and right; VLBA images of components B and C. All VLBA maps have restoring beams of 2.8×1.6 mas^2 in PA 2° and lowest contour levels of 1 mJy. Contours in all images increase logarithmically by factors of 1.41.

Table 2. Positions of components, including the lensing galaxy G, and flux densities at various frequencies for the observations given in Table 1 (M95 refers to the 1995 March 09 MERLIN observation and M96 to the MERLIN observation of 1996 November 15). The positions are based on the MERLIN 5-GHz deep image except for G which is based on the *HST* 814-nm image. Errors in positions are about 10 mas (although relative errors are much smaller, of the order of 1 mas for components A, B and C), and in fluxes about 5 per cent except for the MERLIN and *HST* images where they are rather higher (about 10–15 per cent). Fluxes from the *HST* images have been derived by use of TinyTim point-spread functions (Krist 1995), subtracting them until by eye the emission from the image is removed. The optical fluxes for the galaxy are those in a 2×1 arcsec^2 elliptical aperture; the integrated fluxes are 17.5 and 8.4×10^{-18}erg cm^{-2}s^{-1}Å^{-1} for the 555-nm and 814-nm filters respectively.

Cpt	Right ascension (J2000)	Declination (J2000)	Flux (5 GHz) M95,mJy	Flux (5 GHz) M96,mJy	Flux (5 GHz) VLBA,mJy	Flux (15 GHz) mJy	Flux (814 nm) 10^{-18}erg cm^{-2}s^{-1}Å^{-1}	Flux (555 nm) 10^{-18}erg cm^{-2}s^{-1}Å^{-1}
A	07 16 3.577	47 08 50.15	15.3	10.5	10.7	15.6	0.87	1.02
B	07 16 3.582	47 08 49.99	14.1	8.5	8.8	11.6	0.33	0.33
C	07 16 3.656	47 08 49.48	6.9	4.7	3.6	5.9	0.38	0.40
D	07 16 3.691	47 08 50.61	2?	0.9	<1.0	1.1	0.02?	–
G	07 16 3.653	47 08 50.30	–	–	–	–	11.7	4.9

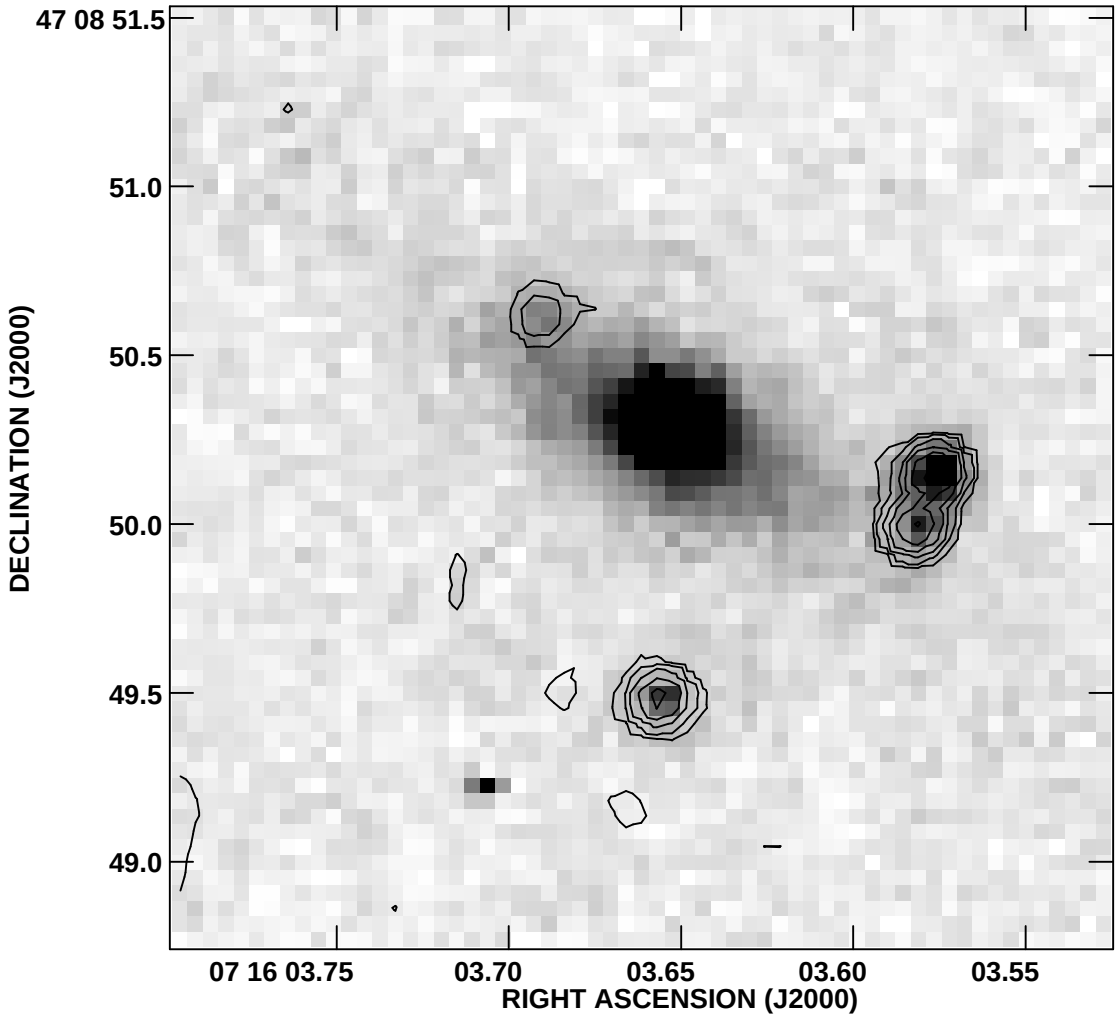

Figure 2. *HST* 814-nm image, in grey-scale, with MERLIN 5-GHz contours overlaid. The images A–D are identified in the first panel of Fig. 1. Note the clear detection of the lensing galaxy and the good coincidence of the radio and optical images of the background quasar.

This yields an absolute magnitude M_V of -21.6.[1] This puts the lensed object of B0712+472 among the very lowest-power flat-spectrum quasars in the PR/CJ faint flat-spectrum surveys (Taylor et al. 1994; Henstock et al. 1995). The problem is made worse by the likely factor of > 10 magnification appropriate for four-image lensing. We argue in the next section that this cannot be completely accounted for by reddening.

[1] $H_0 = 50\,\mathrm{kms}^{-1}\,\mathrm{Mpc}^{-1}$, $q_0 = 0.5$, and assuming $z = 1.33$ for the lensed object (see Section 3).

2.3 Comparison of radio and optical images

Comparison of the radio and optical flux density ratios reveals a

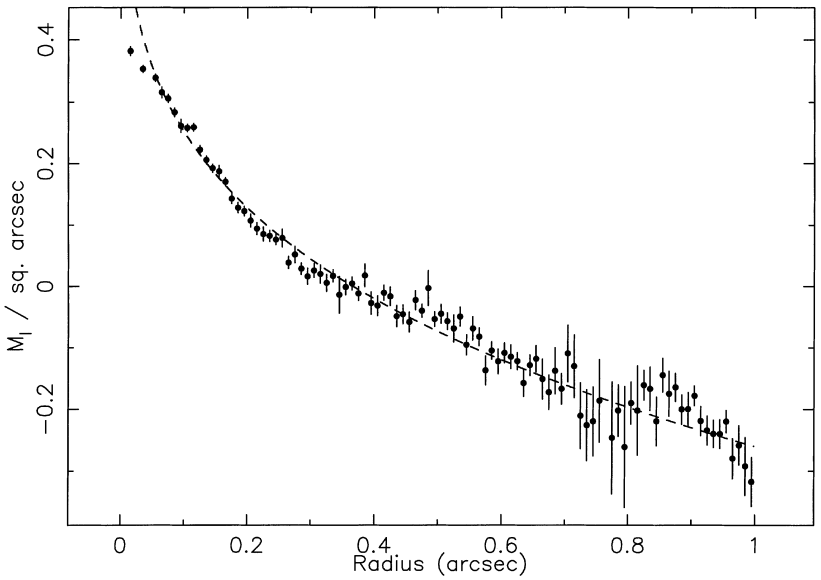

Figure 3. Profiles, on a magnitude scale relative to the central brightness, of the B0712+472 lens galaxy, plotted against r in arcsec. The dashed line represents a $r^{1/4}$ law fit. An exponential disc fits only from 0.3 arcsec outwards.

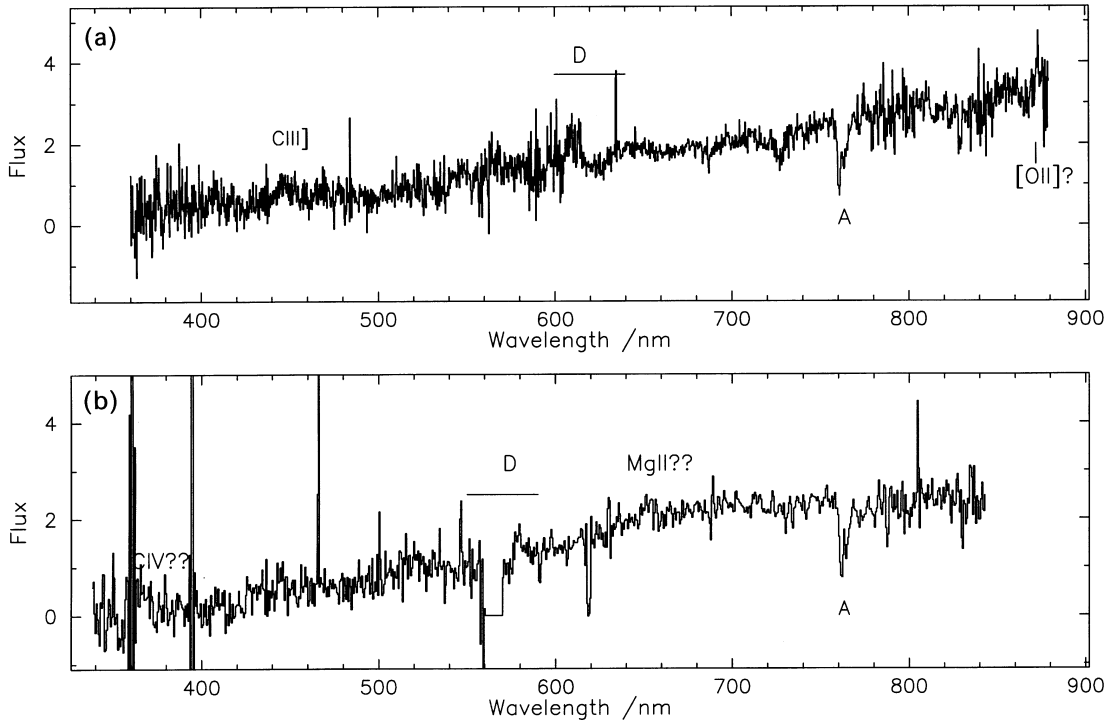

Figure 4. WHT spectra of B0712+472, taken on two different occasions (top, 1995 Dec 23; bottom, 1995 Dec 22; see text). Areas affected by the dichroic cut are marked by a D. All flux scales are arbitrary.

major anomaly; the ratio of the flux density of B to the other components is different in the radio and the optical (Table 2). The flux density of component B is twice that of C and about 75 per cent of that of A in the 15-GHz image. In the optical images it is fainter than C and about one-third of A. The apparent lack of relative variability between the four images in our radio maps, and the fact that theoretically, the arrival times at the observer for light from A and B would be expected to have a negligible time delay between them (a few days), suggest that other factors are responsible for the radio/optical differences. A possibility is that B is reddened. This appears plausible, given that the line of sight to it passes through the major axis of the lensing galaxy. The observed flux ratio B/C then implies $A_V \sim 1$ mag at B, assuming C to be unreddened. Assuming a Galactic reddening law (e.g. Howarth 1983) this implies an extinction of about 0.6 mag at 814 nm for B compared to C. This is a problem given the lack of difference in the ratios of *V/I* flux between A, B and C, although a slight reddening can be accommodated by the numbers in Table 2. To be completely consistent with a Galactic reddening law one would expect the 814-nm flux of B to be about 30 per cent higher, i.e. about 0.44×10^{-18} erg cm^{-2} s^{-1} Å^{-1}. Reddening is a possible explanation for the observed fluxes despite this discrepancy.

Another interesting possibility is that observations of B in the *V* and *I* bands could be affected by microlensing by stars in the lensing galaxy (Chang & Refsdal 1979; Kayser, Refsdal & Stabell 1986). The size of the optical counterpart of a quasar is expected to be less than a microarcsec, the scale of the Einstein radius of a star (microlens) at the distance of a typical lensing galaxy. The optical source thus appears pointlike to microlenses, and can be significantly magnified or demagnified by them: however, the radio source size is bigger and the radio flux is not subject to microlensing. For B0712+472, in the absence of microlensing, one expects on theoretical grounds that A and B should be the brightest images in the system given their proximity to each other. This is indeed the case in the radio, despite observations of an overall variability. In the optical, the fact that B is only the third brightest image combined with the near absence of any colour differences between A, B and C, points to the possibility that microlensing, which is to first order an achromatic effect in the optical, has dimmed B to about a third to a half of its radio brightness. While the proximity of B to the plane of the lensing galaxy makes it susceptible to microlensing, nearby A samples a sufficiently distinct line of sight through the lens that it can remain relatively unaffected, as is evidenced by the similarity of the C/A flux density ratios in both radio and optical observations in Table 2. Since the typical time-scales of microlensing events tend to be of the order of years to tens of years, temporal variations of the flux density of B may not be detected for a few years. However, *HST K*-band observations of the system should be able to discriminate whether dimness of B in the optical is a result of reddening or microlensing.

3 OPTICAL SPECTRA

Spectra were taken of B0712+472 on two occasions using the ISIS spectrograph on the William Herschel Telescope, La Palma (Fig. 4). Blue and red spectra were obtained with a total useful wavelength range from 360 to 900 nm using a dichroic cutting at 580 nm, a slit position angle of 150° and an integration time of 1 h (1995 December 23) or a 610-nm dichroic, a slit position angle of 148° and an integration time of 30 min (1995 December 22).

The signal-to-noise ratio of both spectra is not high. The only line that can be seen with reasonable certainty is a broad line at 445 nm. We provisionally identify this as CIII] at redshift ∼1.33. If it were CIV at redshift 1.89 we would expect to see CIII] at 550 nm and there is no line at this wavelength. Similarly, if it were MgII at redshift 0.59, we would expect to see [OIII] at 800 nm and again there is no line at this wavelength. The redshift of 1.33 is supported by marginal evidence for MgII at ∼650 nm on the 1995 December 22 spectrum although unfortunately this wavelength is affected severely by the dichroic cut on the other spectrum. There is also marginal evidence for [OII] at 872 nm on the 1995 December 22 spectrum which would support a redshift of ∼1.33.

There are no clear features which might allow a determination of the galaxy redshift, despite the fact that our *HST* imaging observations show that galaxy light will dominate the spectrum in both *V* and *I* band; in particular neither the Ca K and H lines nor the 4000-Å break is clearly seen. There is a hint of Ca H and K at ∼557nm, although this wavelength is contaminated by a strong sky-line; the implied redshift of 0.40 places the MgI absorption band close to a small atmospheric absorption band. Higher signal-to-noise spectra will be needed to resolve this matter.

4 LENS MODELLING

We have modelled B0712+472 as a system of four gravitationally lensed images. Image positions and flux density ratios between pairs of images are taken from the 1996 5-GHz MERLIN map, which has the most reliable information on image D among our observations and is unaffected by microlensing or reddening. Positional uncertainties are calculated as the beamwidth divided by twice the signal to noise ratio for each of the images, with values 0.12, 0.15, 0.27 and 1.38 mas for A, B, C and D respectively. We ignore for the present the possibility that the flux density ratios derived from these observations are altered by significant relative variability between the radio images: the 5-GHz data in Table 2 suggest that the radio flux density ratio C/A could vary by about 25 per cent between epochs. However, fitting the images with Gaussian profiles indicates that errors of fit are of the order of about 5 per cent for images A, B and C and 20 per cent for image D; these enter into calculations of the image flux density ratios.

A brief outline of the modelling approach and code is given here; a detailed description is to be found in Nair (in preparation). The lens galaxy is described by a parametrized oblate spheroid with mass density distribution, ρ, of the form

$$\rho(m) = \rho_0/[1 + (m/a)^2], \quad (1)$$

where a is the scalelength of the mass distribution, and $m^2 = x^2 + y^2 + z^2/(1 - e^2)$ is the square of the semi-major axis of an ellipsoidal shell of constant mass density. Equation (1) describes a non-singular (pseudo) isothermal ellipsoid, a convenient representation of the overall mass distribution of the lens galaxy if the lensing properties on arcsec-scale are dominated by its dark halo. The axial ratio of the lens is given by $\sqrt{1 - e^2}$, and it is assumed to be viewed edge-on to reduce the number of parameters considered. This assumption most influences the results of modelling when the lens is assumed to be highly flattened, i.e. disc-like; it appears to be unintrusive in the present case, where the lens is relatively rounder than a bare disc. The orientation of the z-axis, in the plane of the sky, is set by modelling. The lens has six parameters: the coordinates of the lens centre in the lens plane, a mass parameter describing the strength of the lens, its scalelength, ellipticity and the orientation in the plane of the sky. The mass parameter, σ_m, is related to the central density and the scalelength: $\rho_o = 9\sigma_m^2/4\pi G a^2$.

The expression describing the mapping between the multiple image positions and their shared source position, as effected by the lens galaxy, is given in Nair (in preparation); the Jacobian of the inverse mapping (source position ↦ image position) can be defined, and the inverse of its determinant, evaluated at the location of each image, provides the expected geometrical image magnification for a given set of lens model parameters. The ratios of these magnifications with respect to the brightest image, A, yield a set of model-predicted image flux density ratios. In general, for a given set of lens parameters, the individual image positions do not map on to precisely the same source position. Hence the aim of the modelling process is to find that set of lens parameters for which the mismatch in recovered source positions is minimal, subject to the constraint that the model must provide image flux density ratios that match the observed values. Our modelling process thus follows the basic approach of Kayser & Schramm (1988). A numerical code which employs a penalty function to enforce the requirement is described in Nair (in preparation).[2] Minimization is achieved using the method of simulated annealing. An initial constraint applied to

[2]We do not follow the more sophisticated approach of Kochanek (1991) wherein the source plane mismatches are translated to the image plane and compared with the observational uncertainties, for reasons described in Nair (in preparation).

Table 3. Details of the lens model: for the four images of B0712+472, the absolute magnifications, predicted flux density ratios with respect to image A, the image parities and the model-recovered source locations $[\delta(\mathrm{RA}), \delta(\mathrm{Dec.})]$ with respect to the lens centre. In parentheses beside each flux density ratio is the observed value, with uncertainties as estimated from the errors of fit. The source positions are mean values for all back-projected images; the standard deviations are also given. The lens centre is 0.743 arcsec east and 0.087 arcsec north of component A.

Cpt	Model Magn.	Flux (obs.) Ratio	parity	Recovered Source Pos.(mas)
A	26.0	1.00 .(1.00 ± 0.00)	+1	δRA : −0.057 ± 0.007
B	22.4	0.86 .(0.81 ± 0.07)	−1	δDec : −0.064 ± 0.003
C	6.8	0.26 .(0.45 ± 0.07)	+1	
D	2.5	0.10 .(0.09 ± 0.21)	−1	

the penalty function is that the image parities predicted by the model should conform to the set of expected parities; this easily achieved constraint ceases to be important very quickly in the minimization process and is employed chiefly to ensure that the image configurations investigated are physically possible ones. The total number of active constraints operating for most part is $3(4-1) = 9$, for the four images. $2(4-1)$ of these come from considering that the recovered source positions must coincide in the plane of the sky, and the remaining three come from the image flux density ratios. The problem is overconstrained as there are only six parameters, of which one, the scalelength, is restricted to an upper limit of 0.0003 arcsec to stabilize the problem for this particular system. In view of the fact that positions are more accurately determined than the flux density ratios, a weighting is applied to permit greater laxity in matching the latter as compared with the former (in the present case, the 'goal' set for source positions to match is to within 1 mas, and that for the ratio of model to observed flux density ratios is to within 0.05). Note that the lens parameters enter non-linearly in the penalty function.

There are two sources of error that can be distinguished for the best-fitting model that emerges from this process. One represents the level of the idealized lens model's inability to match the observations, even if there were no uncertainties in determining the observational inputs. This manifests as a spread in recovered source positions for the best-fitting lens model (owing to the relative weightings, this usually dominates over mismatches in flux density ratios). The second source of error is the spread in input image positions and flux density ratios arising as a result of observational uncertainties. The contributions of these two errors are not independent, and the most appropriate method of determining the model uncertainties that arise as a result appears to be through a Monte Carlo exercise. We quote 90 per cent confidence intervals on the estimated model parameters from this exercise by considering both the positional uncertainties and those arising from errors of fitting in the case of the image flux density ratios. Note that the observed positional uncertainties of ∼0.1–1.4 mas typically translate to several tens of microarcsec in the source plane, given the image magnifications in Table 3; that the lens model does not fit to within the observational errors is not surprising, especially considering the simplified ellipsoidal mass model used in place of substructure within the actual lens (disc, spheroid, dark matter). However, more detailed mass modelling will require better observational input to characterize the luminous matter distribution, reducing the number of parameters that such a model would otherwise require. The

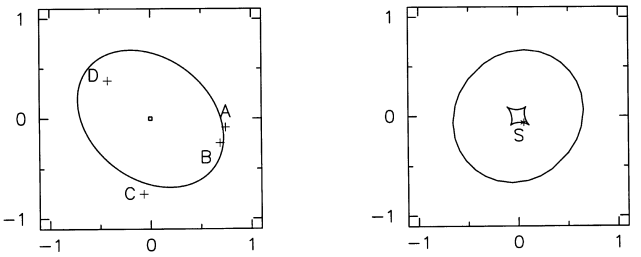

Figure 5. Lens model for B0712+472. (a) Image plane critical curves for the lens model, with the observed image positions superposed. The lens is centred at (0,0). (b) The corresponding source plane caustics for the model. The position of source is marked.

parameters of the best-fit model are as follows (90 per cent confidence intervals in brackets):

Scalelength a: 300 μas (119, 300)μas.
Eccentricity e: 0.66(0.43, 0.74).
Mass parameter σ_{m}: 78.4(74.1, 81.4)km s^{-1}.
PA of lens major axis: 50.6°(49.9°, 54.4°) (cf. observation: 60 ± 5°).
Lens centre (RA, Dec. with respect to image A): (743 ± 33E, 87 ± 50N) mas [cf. observation: (786 ± 20E, 150 ± 20N) mas].

The circular velocity of the lens galaxy can be calculated from the lens mass profile (equation 1) and the model parameters (equation 4 in Nair, in preparation): This yields a value of $214 \times \sqrt{D_s/D_{ls}}$ km s^{-1} for the circular velocity at large radii (asymptotic value). The critical curves and caustics for the model are shown in Fig. 5. The oblate spheroidal lens model has an axial ratio ($b/a = \sqrt{1-e^2}$) of 0.75 (0.67,0.90), to be contrasted with that of the observed light distribution of 0.5 to 0.6. Thus the light distribution is flattened relative to the mass distribution as inferred by modelling, but it does have the same position angle. The model lens centre appears closer to image A than the observations would suggest, though consistent within the combined observational and modelling errors. The apparent shift may well be an artefact of the near-singular lens mass profile employed in the model, as perhaps is the lesser flattening; a mass model with a larger scalelength would be both flatter and more asymmetrically disposed with respect to the circle of images. The closeness of the observed and model values of the PA of the major axis of the lens in the plane of the sky is actually quite surprising, and it remains for a refined model to be made when there is an adequate knowledge of the temporal behaviour of the image flux density ratios, to ascertain how far this coincidence is borne out. That these values are in conformity with each other appears to be the best argument in support of the picture that the lensing is dominated by a single lens galaxy. It is worth remarking that the confidence interval on estimated lens parameters is significantly larger for certain parameters in our Monte Carlo exercise than the typical values of a few per cent to be found in 'formal' estimates in the literature so far.

5 CONCLUSION

We have found another radio-loud, four-image lensed system in the first phase of the CLASS survey. The lensed object is weak (∼30–40 mJy at GHz frequencies), and has a probable redshift of 1.33. There is evidence for some radio variability, but no clear evidence for relative variability in component flux ratios. The lensing galaxy is detected; it is of unknown redshift (though

probably between 0.3 and 0.7) and appears flattened. One of the images, B, is either reddened or demagnified by microlensing in the optical; future observations should be able to identify which of the two possibilities dominates. The lensed object is underluminous compared to other radio-loud quasars.

The system B0712+472 is one of five multiply imaged quasars found in the JVAS/CLASS survey for which the lenses have been identified to be of type S0 or later, out of a total of 10 candidate systems (Jackson et al. 1997). This is a remarkable string of discoveries; theoretical treatments of the statistics of lensing (e.g. Turner, Ostriker & Gott 1984) have so far suggested that galactic-scale lensing is dominated by E/S0 galaxies. The JVAS/CLASS survey is a radio survey and is not subject to any obvious selection bias, so this result is surprising. We argue elsewhere (Jackson et al. 1997) that lenses such as B0712+472 may be evidence for flattening of dark matter haloes in spiral galaxies.

ACKNOWLEDGMENTS

MERLIN is operated as a National Facility by NRAL, University of Manchester, on behalf of the UK Particle Physics & Astronomy Research Council. The William Herschel Telescope is operated by the Royal Greenwich Observatory on the island of La Palma at the Spanish Observatorio del Roque de los Muchachos of the Instituto de Astrofísica de Canarias. The VLA and VLBA are operated by Associated Universities for Research in Astronomy Inc. on behalf of the National Science Foundation. This research used observations with the Hubble Space Telescope, obtained at the Space Telescope Science Institute, which is operated by Associated Universities for Research in Astronomy Inc. under NASA contract NAS5-26555. One spectrum was obtained as part of the La Palma telescopes international time project 'The radio universe at low flux density levels' allocated by the Comite Cientifico Internacional, and the other by the WHT service programme. All spectra were processed using the National Optical Astronomy Observatories IRAF package. We thank the pulsar group at Jodrell Bank for the use of their computing facilities. This research was supported by European Commission, TMR Programme, Research Network Contract ERBFMRXCT96-0034 'CERES'.

REFERENCES

Abraham R. G., Valdes F., Yee H. K. C., van den Bergh S., 1994, ApJ, 432, 75
Abraham R. G., van den Bergh S., Glazebrook K., Ellis R. S., Santiago B. X., Surma P., Griffiths R., 1995, ApJS, 107, 1
Abraham R. G., Tanvir N. R., Santiago B. X., Ellis R. S., Glazebrook K., van den Bergh S., 1996, MNRAS 279, L47
Chang K., Refsdal S., 1979, Nat, 282, 561
Condon J., Broderick J., Seielstad G. A., 1989, AJ, 97, 1064
Driver S. P., Windhorst R. A., Griffiths R. E., 1995, ApJ, 453, 48
Fukugita M., Shimasaku K., Ichikawa T., 1995, PASP, 107, 945
Gregory P. C., Condon J. J., 1991, ApJS, 75, 1011
Henstock D., Browne I. W. A., Wilkinson P. N., Taylor G. B., Vermeulen R. C., Pearson T., Readhead A. C. S., 1995, ApJS, 100, 11
Howarth I., 1983, MNRAS 203, 301
Jackson N. et al., 1995, MNRAS, 274, L25
Jackson N. et al., 1998, ApJ, submitted
Katz C. A., Hewitt J. N., 1993, ApJ, 409, L9
Kayser R., Refsdal S., Stabell R., 1988, A&A, 191, 39
Kayser R., Schramm T., 1988, A&A, 191, 39
Kochanek C. S., 1991, ApJ, 382, 58
Krist J., 1995, TinyTim Users' Manual. STScI, Baltimore
Myers S. et al., 1995, ApJ, 447, L5
Patnaik A. R. et al., 1992, MNRAS, 259, 1P
Shepherd M. C., Pearson T. J., Taylor G. B., 1995, BAAS, 27, 903
Sykes C. M. et al., 1998, MNRAS, in press
Taylor G. B., Vermeulen R. C., Pearson T., Readhead A., Henstock D., Browne I. W. A., Wilkinson P. N., 1994, ApJS, 95, 345
Turner E. L., Ostriker J. P., Gott J. R., 1984, ApJ, 284, 1

This paper has been typeset from a TEX/LATEX file prepared by the author.